*Progress In Electromagnetics Research C, Vol. 63, 85–94, 2016*

# A Dual-Band Meandered Dipole Antenna for Medical Telemetry Applications

**Johnny Ung and Tutku Karacolak**

**Abstract**—The aim of this study is to present a dual-band antenna for Wireless Medical Telemetry Service (WMTS) applications. The antenna covers all three frequency bands 608–614 MHz, 1395–1400 MHz, and 1427–1432 MHz, and is intended for continuous health monitoring of patient's vital parameters. The designed antenna consists of a meandered dipole antenna and a superstrate layer to preserve the biocompatibility of the structure. It has a compact size with dimensions 17.6 mm × 12 mm × 2.54 mm. The measured −10 dB bandwidths are found to be 16.3% for the lower frequency band and 10.6% in the upper frequency band. The antenna is *in vitro* tested in a tissue mimicking solution.

## 1. INTRODUCTION

The design of implantable medical devices has been critical in recent years for medical telemetry. In the practice of medicine, there are many diagnostic and therapeutic applications in which a medical device is implanted within a patient [1]. Often, communication between the device and external equipment is necessary, and this is done wirelessly using an implantable antenna and an external receiver. This necessitates the design of efficient implantable antennas for overall system reliability. There are many challenges in designing implantable antennas such as antenna size, impedance matching in an electrically lossy environment, biocompatibility, and limitations on specific absorption rate (SAR). In addition, bandwidth needs to be improved to make the antennas robust and reliable against changes in the biological environment.

To tackle these challenges, various microstrip antenna configurations have been proposed including spiral, serpentine, circular and square stacked planar inverted-F antennas [2–6]. Dipoles and loop antennas are also used for certain biotelemetry applications [7, 8]. Several frequency bands are reserved by Federal Communications Commission (FCC) to regulate spectrum usage for medical implant communications [9]. The Medical Device Radiocommunications Service (MedRadio) band (401–406 MHz) is the most commonly used medical band, especially for diagnostic and therapeutic purposes as well as on-body devices. Industrial, Scientific, and Medical (ISM) bands (433, 915, 2450, 5800 MHz) have also been preferred for some biotelemetry applications. Finally, FCC approved the Wireless Medical Telemetry Service (WMTS) band (608–614, 1395–1400, and 1427–1432 MHz) mainly for remote monitoring of a patient's physiological parameters (glucose level, blood pressure, body temperature, heart rate, chemical concentrations, etc.). Since then, several antennas are designed utilizing WMTS bands. In [10], an S-shaped PIFA is proposed for biotelemetry in MedRadio, WMTS, and ISM bands. Similarly, a tri-band Egret-Beak shaped implantable antenna is presented operating at the same frequency ranges [11]. A meander line shaped patch antenna and a CPW fed spiral antenna are demonstrated in [12] and [13], respectively. Both designs are wideband and operate at 1395–1400 and 1427–1432 WMTS bands.

The objective of this study is to design an implantable dual-band antenna for WMTS (608–614 MHz, 1395–1400 MHz, 1427–1432 MHz) biotelemetry applications. The proposed design is a meandered dipole

*Received 26 January 206, Accepted 9 April 2016, Scheduled 19 April 2016*
* Corresponding author: tutku.karacolak@wsu.edu (Tutku Karacolak).
The authors are with the School of Engineering and Computer Science, Washington State University Vancouver, Washington, USA.

antenna with superstrate. The antenna's first operating band covers the 608–614 MHz WMTS band, while the second operating band covers both the 1395–1400 MHz and 1427–1432 MHz bands. The proposed antenna is compact, with dimensions $17.6 \times 12 \times 2.54\,\text{mm}^3$. To the best of our knowledge, this is the first design utilizing all three WMTS bands.

In this study, we first discuss the design and optimization of the antenna using numerical simulation techniques. The antenna is then fabricated and tested in a tissue mimicking gel that approximates the electrical properties of human skin. Measurement and simulation results will be presented including impedance matching, radiation patterns, gain, and SAR distribution.

## 2. ANTENNA DESIGN

The antenna is designed in two major stages: Initial design and parametric analysis.

### 2.1. Initial Design

An initial draft of the antenna design is first simulated using ANSYS HFSS. To obtain dual-band operation with compact size, a meandered dipole design is considered. The geometry of the antenna design is shown in Fig. 1(a). The meander of the lines reduces the overall volume of the antenna while maintaining good radiation characteristics. It allows for increasing the electrical length of the radiator without increasing the overall size of the antenna to lower the first resonance frequency to 608–614 MHz. Basic design variables for a meandered line dipole include the width of all lines and the length of each line segment before. The proposed design uses a superstrate which is bonded to the substrate. Since all conductors are placed at the surface where the substrate and superstrate meet, there are no conductors on the outside of the antenna which would make contact with the surrounding tissue when implanted. This means that it is possible to use a non-biocompatible conductor for the antenna, if desired, assuming that a biocompatible substrate and superstrate are chosen. Alumina ($\varepsilon_r = 9.4$, $\tan\delta = 0.006$) is chosen as the substrate and superstrate material for its biocompatibility and relatively high permittivity for additional size reduction. The antenna is modeled in simulation within a skin phantom using frequency dependent dielectric properties of human skin found in literature [14, 15] (see Fig. 1(b)).

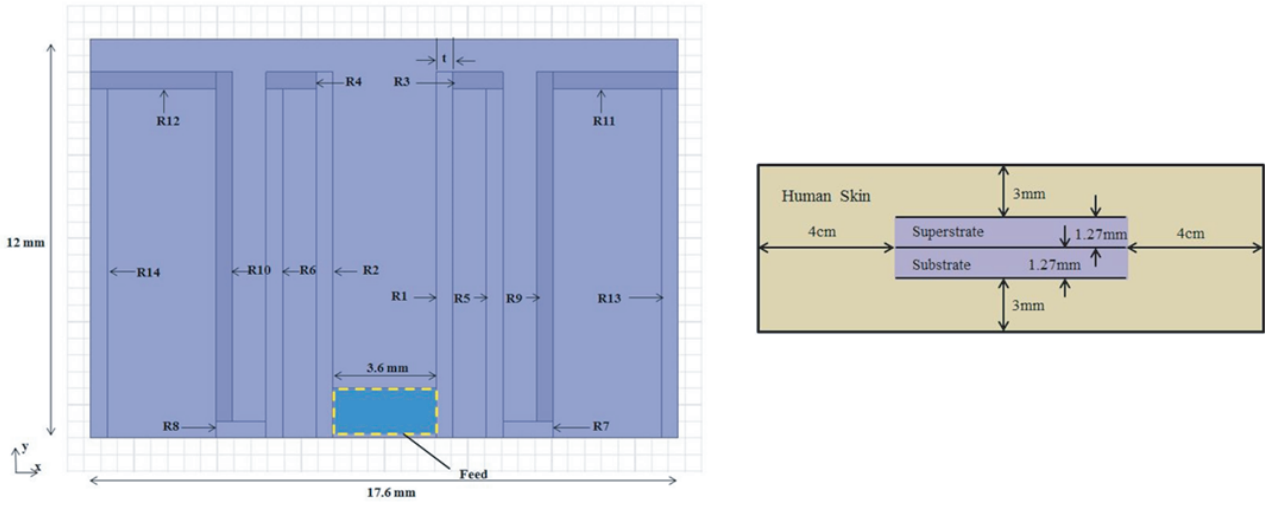


(a) (b)

**Figure 1.** (a) Top view of antenna with conductor parameters, and (b) side view of the antenna.

### 2.2. Parametric Analysis

The meandered dipole antenna is optimized by way of parametric analysis. The goal of the analysis is to improve impedance matching in the WMTS bands while also improving bandwidth. The length of

**Table 1.** Optimized dimensions of the antenna.

| Conductor | Parameter name | Length (mm) |
|---|---|---|
| R1 & R2 | R1y, R2y | 11.0 |
| R3 & R4 | R3y, R4y | 1.5 |
| R5 & R6 | R5y, R6y | 10.5 |
| R7 & R8 | R7y, R8y | 1.5 |
| R9 & R10 | R9y, R10y | 10.5 |
| R11 & R12 | R11y, R12y | 3.75 |
| R13 & R14 | R13y, R14y | 10.5 |
| Width of all conductors, $t$ | $t$ | 0.5 |

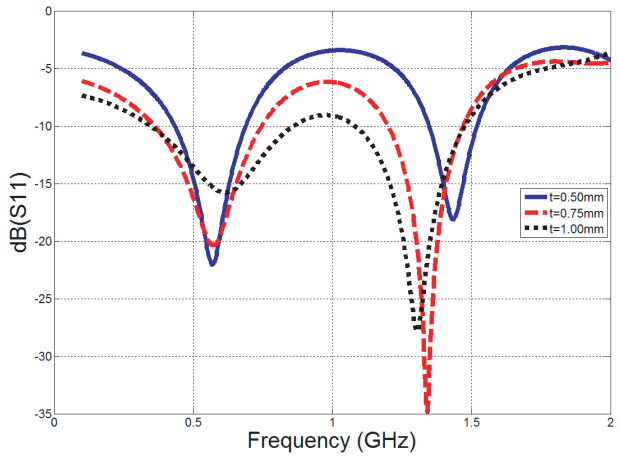


**Figure 2.** The return loss while sweeping the width of all conductors $t$.

each conductor is assigned as a parameter (Fig. 1(a)). The width of all conductors is also assigned as a parameter, $t$. The resulting optimized dimensions of the radiating conductors are shown in Table 1. Sweeps of a few of the parameters with the largest impact on return loss are shown in Fig. 2, Fig. 3(a), and Fig. 3(b). Fig. 2 gives the return loss of the antenna while varying the width of all of the conductors. It is seen that as the width increases, the impedance matching in the first band degrades while the matching in the second band improves. Also, as the width increase the resonant frequency of the first band increases, while the resonant frequency of the second band decreases. We have determined $t = 0.5\,\text{mm}$ as the optimum dimension for the conductor width. Fig. 3(a) gives the return loss while sweeping several parameters. Here, the conductors R5, R6, R9, R10, R13, and R14 are all given a length equal to the length of R1 less 0.5 mm. R2 is given the same length as R1, and R1 is swept. It is seen that as the length of all of the conductors increase, the return loss in both bands improves and shifts to lower frequencies. Fig. 3(b) gives the return loss of the antenna while sweeping the length of the conductor R11. The trend observed is that as the length of R11 increases, the return loss in both bands improves and shifts to lower frequencies. It is seen that the increase in conductors' physical and electrical lengths in Figs. 3(a) and 3(b) results in a longer current path that lowers the resonance frequencies of both bands and shifts towards left.

The optimized return loss of the antenna is given in Fig. 4(a). The optimized antenna has $-10\,\text{dB}$ bandwidths of 45.8% and 12.4% in the lower and upper operating frequency bands, respectively. Fig. 4(b) shows the return loss comparison of the antenna when simulated using alumina and Rogers RO3210 substrates. It is seen that antennas of both substrates have very similar responses, with nearly identical lower frequencies and only a small shift in the upper frequency band. Both materials have

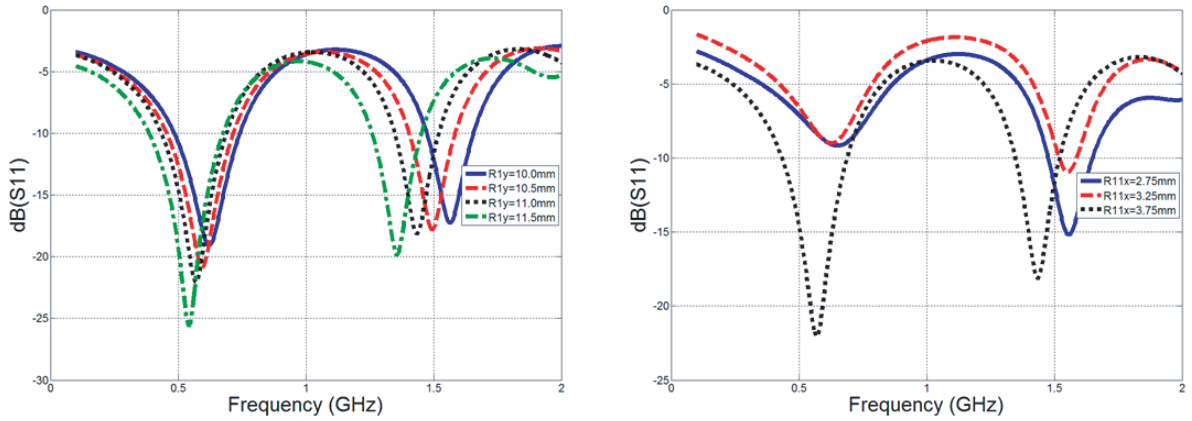


(a) (b)

**Figure 3.** (a) The return loss while sweeping the length of the conductors R1, R2, R5, R6, R9, R10, R13, and R14 and (b) the return loss while sweeping the length of the conductor R11.

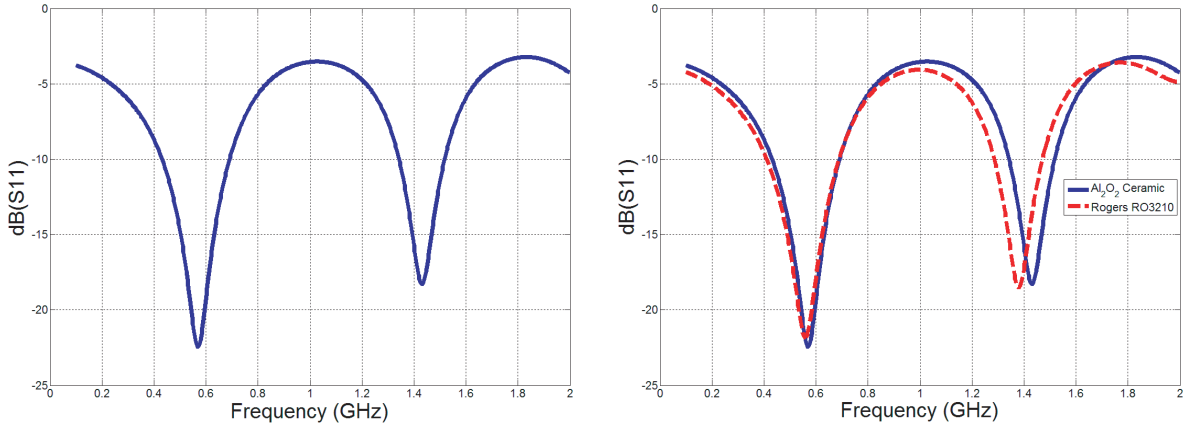


] (a) (b)

**Figure 4.** (a) The return loss of the antenna with optimized topology, and (b) the return loss of the antenna on alumina and Rogers RO3210 substrates.

similar dielectric properties, and as shown in [16] Rogers RO3210 substrate ($\varepsilon_r = 10.2$, $\tan\delta = 0.003$) may be substituted for an alumina substrate for *in vitro* performance characterization. As a proof of concept for the antenna performance, Rogers RO3210 substrate is used for the testing of the antenna in this study.

## 3. IN VITRO MEASUREMENTS

The antenna of Fig. 1(a) is fabricated. To fabricate the antenna, the meandered dipole geometry is milled out of the substrate material. After milling, the superstrate is bonded to substrate. The fabricated antenna and the substrate layer are shown in Figs. 5(a) and 5(b), respectively. To test the antenna *in vitro*, a simple skin mimicking solution is prepared using a recipe of deionized water and sugar [17]. The electrical properties are measured by the Agilent 85070E dielectric probe kit. The skin mimicking solution makes a fair approximation of the relative permittivity and conductivity of human skin in the WMTS bands. Measured values at 600 MHz were $\varepsilon_r = 46.8$ and $\sigma = 0.42\,\mathrm{S/m}$ ($\varepsilon_r = 43.6$, $\sigma = .76\,\mathrm{S/m}$ in literature). Measured values at 1.4 GHz were $\varepsilon_r = 38.4$ and $\sigma = 1.18\,\mathrm{S/m}$ ($\varepsilon_r = 39.7$, $\sigma = 1.03\,\mathrm{S/m}$ in literature). The dielectric values of the solution match those values found in literature

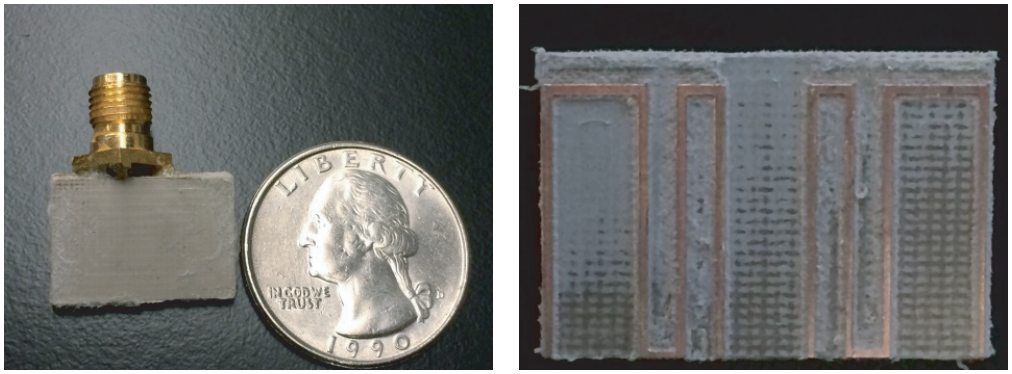


(a) (b)

**Figure 5.** (a) Fabricated antenna and (b) antenna substrate.

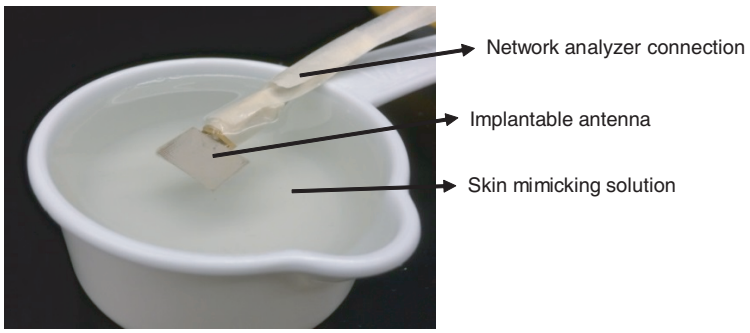


**Figure 6.** Test setup showing the antenna submerged in the skin mimicking solution.

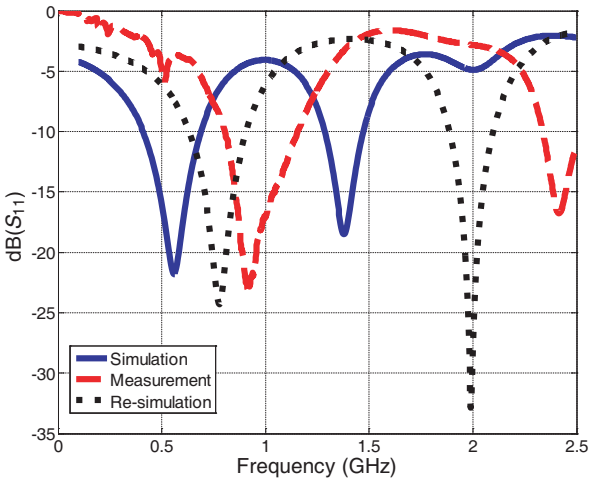


**Figure 7.** The measured and simulated return loss of the antenna.

fairly well. The antenna is submerged in the skin mimicking solution for testing as shown in Fig. 6. The return loss measurement is performed using an Agilent N5230C PNA-L network analyzer.

Figure 7 shows a comparison between the measured and simulated return loss. There is a large frequency shift in both bands of the antenna. This shift may be accounted for with several factors. The simulation does not account for imperfections in the fabrication process. In simulation the superstrate is placed directly on top of the substrate. During actual fabrication, the pins of an SMA coaxial connector sit between the substrate and superstrate and add a gap between the two layers. Adhesive fills this

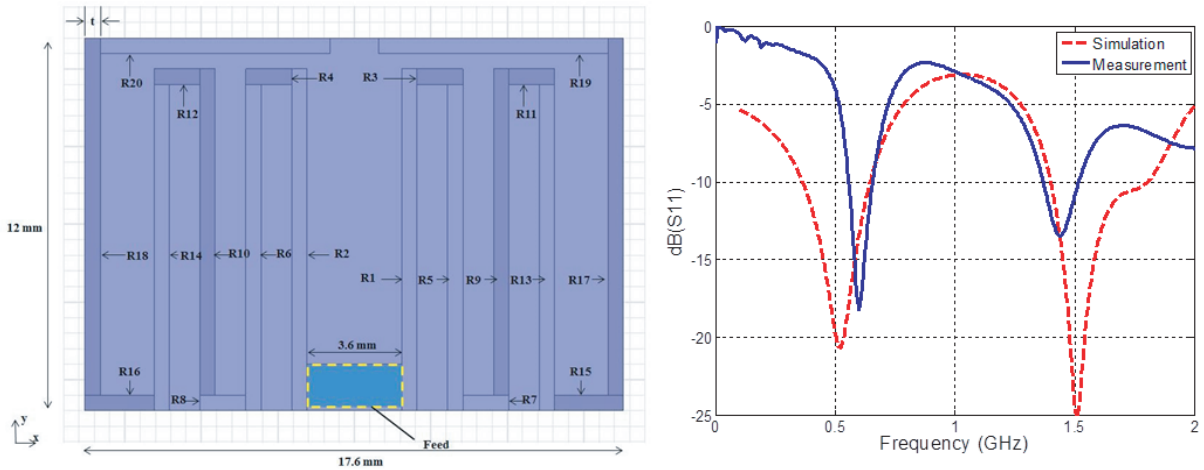


**Figure 8.** (a) Optimized geometry of the second design and (b) Simulated and measured return loss.

**Table 2.** Optimized dimensions of the second design.

| Conductor | Parameter name | Length (mm) |
|---|---|---|
| R1 & R2 | R1y, R2y | 11.0 |
| R3 & R4 | R3y, R4y | 1.5 |
| R5 & R6 | R5y, R6y | 10.5 |
| R7 & R8 | R7y, R8y | 1.5 |
| R9 & R10 | R9y, R10y | 10.5 |
| R11 & R12 | R11y, R12y | 1.5 |
| R13 & R14 | R13y, R14y | 10.5 |
| R15 & R16 | R15y, R16y | 2.25 |
| R17 & R18 | R17y, R18y | 11.5 |
| R19 & R20 | R19y, R20y | 7.5 |
| Width of all conductors, $t$ | $t$ | 0.5 |

gap, but is not accounted for in simulation. This change in dielectric values of from superstrate to adhesive directly above the conductors contributes to the frequency shift. Also, the coaxial connector is soldered manually. It is possible that the connector is slightly shifted from its intended location. These factors are expected to shift the measured response. The design is re-simulated considering some of these effects. We have used sprayable glue 3M77 when bonding the substrate and superstrate layers. A glue layer ($\varepsilon_r = 2$) with an average thickness of 0.5 mm is included in the new simulation model. Also, finite-thickness copper sheets (0.0017 mm) are used to model the meandered dipole instead of zero-thickness and perfectly conducting sheets. The re-simulation is added in Fig. 7. As seen, the new simulation compares closer to the measurement. Taking into account these factors, the antenna is redesigned to obtain good performance in the WMTS bands. The optimized geometry of the redesigned antenna is given in Fig. 8(a). The dimensions for the antenna parameters are given in Table 2. The simulated and measured return loss of the second antenna design is seen in Fig. 8(b). The antenna has measured $-10$ dB bandwidths of 16.3% and 10.6%.

Table 3 compares the dimensions of the proposed antenna with similar designs operating at WMTS bands from the literature. As seen, although the proposed design is slightly larger in size, it operates within all WMTS bands. Covering the lowest WMTS band (608–614 MHz) is the reason for the increase

in antenna size.

Figures 9(a) and 9(b) give plots of the simulated co- and cross-polarized radiated fields of the antenna at 611 MHz in the $\varphi = 0°$ ($yz$ plane) and $\varphi = 90°$ planes ($xz$ plane). Fig. 10(a) and Fig. 10(b) give plots of the simulated co- and cross-polarized radiated fields of the antenna at 1.4 GHz in the $\varphi = 0°$

**Table 3.** Comparison of the proposed antenna with similar designs.

| | [10] | [11] | [12] | [13] | This Work |
|---|---|---|---|---|---|
| WMTS Bands (MHz) | 1427–1432 | 1395–1400<br>1427-1432 | 1395–1400<br>1427–1432 | 1395–1400<br>1427-1432 | 608–614<br>1395–1400<br>1427-1432 |
| Size ($mm^3$) | $10 \times 10 \times 2.54$ | $10 \times 12 \times 1.57$ | $10 \times 12 \times 1.57$ | $8.7 \times 5.05 \times 1.27$ | $17.6 \times 12 \times 2.54$ |

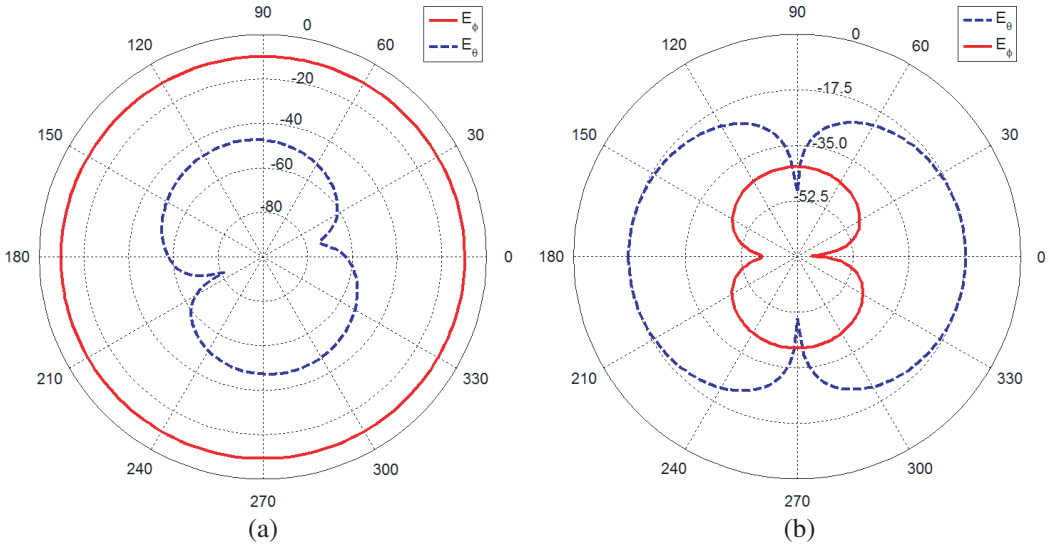


**Figure 9.** Radiation pattern of the antenna at 611 MHz for (a) $\varphi = 0°$ and (b) $\varphi = 90°$ planes.

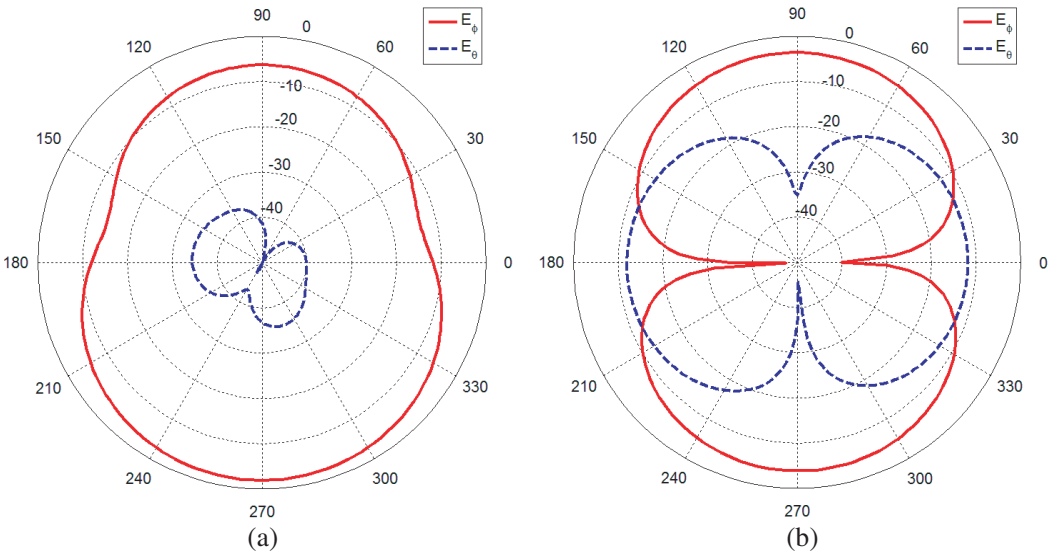


**Figure 10.** Radiation pattern of the antenna at 1.41 GHz for (a) $\varphi = 0°$ and (b) $\varphi = 90°$ planes.

and $\varphi = 90^\circ$ planes. The maximum far-field gain at 611 MHz and 1.4 GHz are calculated to be $-26.5$ dB and $-19.9$ dB. Low gain values can be attributed to the lossy characteristics of biological tissues and these values are consistent with implantable antennas in the literature [2–6].

To ensure human safety, the IEEE standard limits the maximum 1-g average specific absorption rate (SAR) to a value of less than 1.60 W/kg. The 1-g average SAR distribution of the antenna is simulated. SAR values for the bottom of the substrate are found to be larger than for those on the superstrate surface. Fig. 11 gives a plot of the simulated 1-g average SAR on the bottom surface of the substrate at 611 MHz. As seen, the average SAR has a maximum value of 1.6 W/kg at an input power of 4.53 mW. Fig. 12 gives a plot of the simulated 1-g average SAR on the bottom surface of the substrate at 1.4 GHz. The average SAR has a maximum value of 1.6 W/kg at an input power of 3.40 mW. The proposed antenna should be limited to an input power less than 3.40 mW to adhere to the IEEE standard.

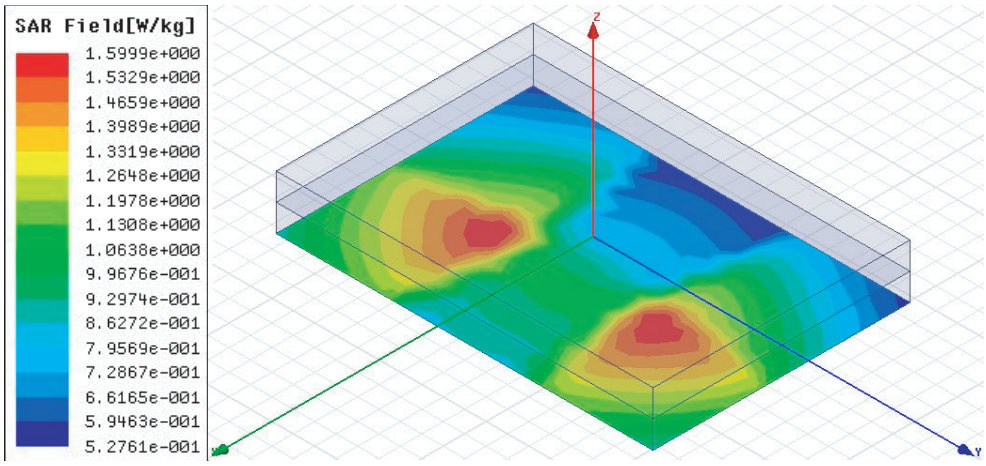


**Figure 11.** The simulated average SAR of the antenna at 611 MHz with 4.53 mW input power.

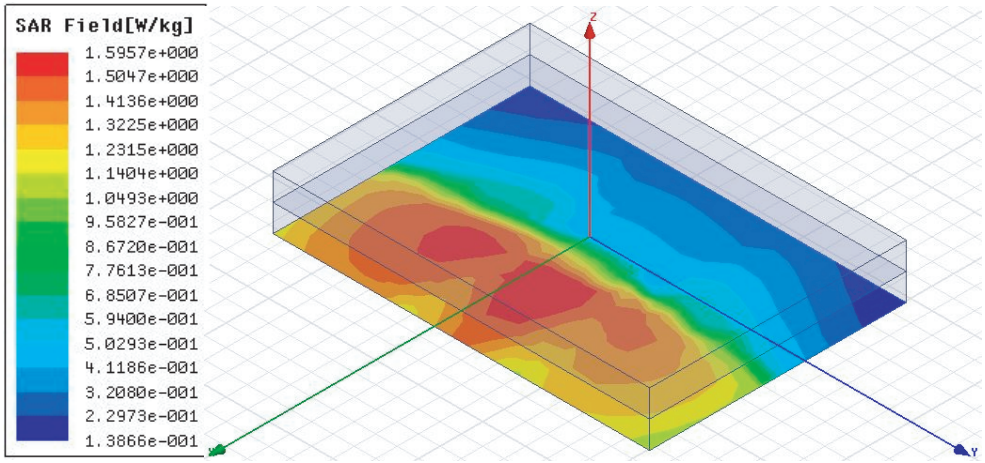


**Figure 12.** The simulated average SAR of the antenna at 1.4 GHz with 3.40 mW input power.

The performance of the dual-band antenna is also simulated in other tissues including brain, muscle, and colon tissue. Fig. 13 gives the performance of the antenna in these other tissues. For these tissues, it is seen that both resonant frequencies of the antenna are shifted slightly to lower frequencies. The antenna still performs adequately in these tissues, but for optimal performance the parameters can easily be optimized for each of the tissues.

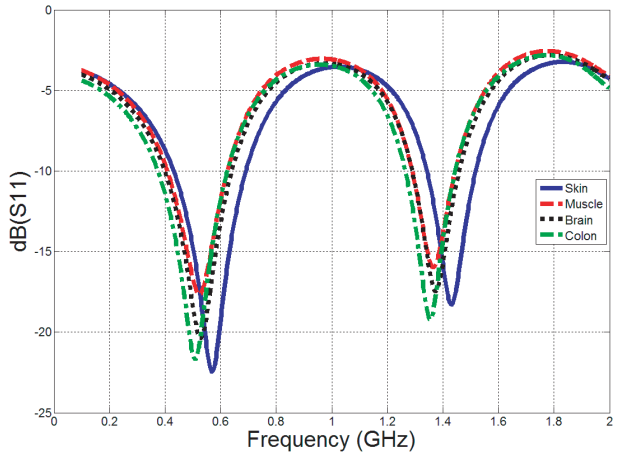


**Figure 13.** Simulated return loss comparison of the antenna in skin, muscle, brain, and colon tissue.

## 4. CONCLUSIONS

An implantable dual-band dipole antenna for WMTS applications is presented. The antenna utilizes a meandered topology with a superstrate layer and has overall dimensions of $17.6 \times 12 \times 2.54\,\text{mm}^3$. The optimized antenna has a measured bandwidth of 16.3% covering the 608–614 MHz WMTS frequency band, and a bandwidth of 10.6% covering the 1395–1400 MHz and 1427–1432 MHz WMTS bands. The antenna has an omnidirectional radiation pattern and allows up to a maximum input power level of 3.4 mW to meet the 1-g average SAR regulation.

## REFERENCES

1. Kiourti, A. and K. S. Nikita, "A review of implantable patch antennas for biomedical telemetry: Challenged and solutions," *IEEE Antennas and Propagation Magazine*, Vol. 54, No. 3, 210–228, 2012.
2. Karacolak, T., A. Zach Hood, and E. Topsakal, "Design of a dual band implantable antenna and development of skin mimicking gels for continuous glucose monitoring," *IEEE Transactions on Microwave Theory and Techniques*, Vol. 56, No. 4, 1001–1008, 2008.
3. Kim, J. and Y. Rahmat-Samii, "Implanted antennas inside a human body: Simulations, designs, and characterizations," *IEEE Transactions on Microwave Theory and Techniques*, Vol. 52, No. 8, 1934–1943, 2004.
4. Soontornpipit, P., C. M. Furse, and Y. C. Chung, "Design of implantable microstrip antennas for communication with medical implants," *IEEE Transactions on Microwave Theory and Techniques*, Vol. 52, No. 8, 1944–1951, 2004.
5. Kiourti, A. and K. S. Nikita, "Miniature scalp-implantable antennas for telemetry in the MICS and ISM bands: Design, safety considerations, and link budget analysis," *IEEE Trans. Antennas Propag.*, Vol. 60, No. 6, 3568–3575, 2012.
6. Merli, F., L. Bolomey, J. F. Zurcher, G. Corradini, E. Meurville, and A. K. Skrivervik, "Design, realization and measurements of a miniature antenna for implantable wireless communication systems," *IEEE Trans. Antennas Propag.*, Vol. 59, No. 10, 3544–3555, 2011.
7. Gosalia, K., M. S. Humayun, and G. Lazzi, "Impedance matching and implementation of planar space-filling dipoles as intraocular implanted antennas in a retinal prosthesis," *IEEE Trans. Antennas Propag.*, Vol. 53, No. 8, 2365–2373, 2005.

8. Chen, Z. N., G. C. Liu, and T. S. P. See, "Transmission of RF signals between MICS loop antennas in free space and implanted in the human head," *IEEE Trans. Antennas Propag.*, Vol. 57, No. 6, 1850–1854, 2009.
9. FCC, Washington, DC, USA, "Federal Communications Commission," 2012 [Online], Available: http://www.fcc.gov.
10. Wu, C., T. Chien, C. Yang, and C. Luo, "Design of novel S-shaped quad-band antenna for medradio/WMTS/ISM implantable biotelemetry applications," *International Journal of Antennas and Propagation*, Vol. 2012, 2012.
11. Shakib, M., M. Moghavvemi, W. Mahadi, and M. Ahmed, "Design of a tri-band implantable antenna for wireless telemetry applications," *IEEE MTT-S International Microwave Workshop Series on RF and Wireless Technologies for Biomedical and Healthcare Applications*, 1–3, London, England, Dec. 8–10, 2014.
12. Shakib, M., M. Moghavvemi, W. Mahadi, and M. Ahmed, "Design of a broadband implantable antenna in the rat for biotelemetry applications," *IEEE MTT-S International Microwave Workshop Series on RF and Wireless Technologies for Biomedical and Healthcare Applications*, 239–240, Taipei, Taiwan, Sept. 21–23, 2015.
13. Ung, J. and T. Karacolak, "A compact ultraminiature coaxial fed antenna for WMTS biotelemetry applications," *Microwave and Optical Technology Letters*, Vol. 57, No. 4, 987–992, 2015.
14. Gabriel, S., R. W. Lau, and C. Gabriel, "The dielectric properties of biological tissues: II. Measurements in the frequency range 10 Hz to 20 GHz," *Phys. Med. Biol.*, Vol. 41, 2251–2269, 1996.
15. Gabriel, C., S. Gabriel, and E. Corthout, "The dielectric properties of biological tissues: I. Literature survey," *Phys. Med. Biol.*, Vol. 41, 2231–2249, 1996.
16. Seran, S., T. Karacolak, and J. P. Donohoe "A small implantable dual band biocompatible antenna for medical wireless telemetry applications," *IEEE APS/USNC/URSI International Symp.*, Orlando, Florida, Jul. 7–12, 2013.
17. Yilmaz, T., T. Karacolak, and E. Topsakal, "Characterization of skin, fat, and muscle mimicking gels for MICS and ISM bands (402–405 MHz and 2.4–2.48 GHz)," *URSI General Assembly*, Chicago, Illinois, Aug. 7–16, 2008.